MATERIALS CHEMISTRY
FRONTIERS

CCS 中国化学会 CHINESE CHEMICAL SOCIETY
ICCAS
ROYAL SOCIETY OF CHEMISTRY

RESEARCH ARTICLE

View Article Online
View Journal | View Issue

Cite this: *Mater. Chem. Front.*, 2022, **6**, 8

A tri-component semiconducting polymer with ultrahigh photothermal conversion efficiency as a biodegradable photosensitizer for phototheranostics†

Yulan Gu,[a] Guoqiang Zhou,*[b] Yujie Zhong,[c] Litao Tan,[c] Zuhui Zheng,[c] Zihan Qiu,[c] Bo Wei,[c] Lei Shen,[c] Jie Yang*[c] and Dengfeng Zou *[d]

Semiconducting polymers usually with high photostability, reactive oxygen species (ROS) generation ability and photothermal conversion efficiency hold tremendous promise for phototherapy. In this study, a biodegradable tri-component semiconducting polymer (NDT) has been designed and synthesized for phototheranostics. NDT nanoparticles (NPs) obtained by nano-precipitation with an ultrahigh photothermal conversion efficiency (65.6%) could be degraded in the presence of hydrogen peroxide in the tumor microenvironment (TME). Such NPs show high phototoxicity towards human cervical cancer cells (HeLa) with laser irradiation as well as negligible dark toxicity. Furthermore, the *in vivo* study demonstrates that tumor growth was inhibited efficiently when mice were injected with NDT NPs, even with low power laser irradiation (0.2 W cm^{-2}). In contrast, higher power density (0.5 W cm^{-2}) led to complete tumor suppression. No side effects were observed towards normal tissues, which was confirmed by the H&E stained pictures of the normal tissues, including heart, liver, spleen, lung and kidney. Further, hematological, liver and renal function parameters indicate the biosafety of NDT NPs.

Received 4th September 2021,
Accepted 4th November 2021

DOI: 10.1039/d1qm01236c

rsc.li/frontiers-materials

Introduction

Over the past decades, cancer has posed a great threat to the health of human beings worldwide, and has become the second leading cause of death, following heart and cardiovascular diseases[1]. Traditional therapeutic methods, such as surgery, radiotherapy, and chemotherapy, may suffer from the disadvantages of non-targeting, severe side effects and a second recurrence of tumor. Phototherapy usually includes the photosensitization process of the surrounding oxygen to convert non-toxic triplet oxygen to cytotoxic reactive oxygen species (ROS), which is the so-called photodynamic therapy (PDT).[2–8] In contrast, non-radiative transition will happen, during which heat will be generated for photothermal therapy (PTT).[9–15] Such a non-invasive therapeutic method holds tremendous promise for cancer treatment.[16–22]

Semiconducting compounds have been universally used in biophotonics, especially in photoacoustic imaging (PA) and photothermal therapy (PTT), due to their excellent thermal stability and high photothermal conversion efficiency.[23–29] Owing to the near infrared (NIR) absorption of such compounds, these compounds are usually capable of achieving deep tissue penetration. Semiconducting compounds are usually utilized in drug delivery and afterglow imaging. For example, Yang *et al.* reported an *in situ* polymerization of perylene diimide hybridized hollow mesoporous organosilica nanoparticles for precision phototheranostics.[26] Among the various semiconducting compounds, heavy atom free compounds are able to minimize the potential dark toxicity of the photosensitizers and thus, reduce the systemic toxicity. For example, Chen *et al.* designed a heavy atom-free compound for efficient singlet oxygen capture and delivery in the dark and hypoxic tumor microenvironment.[27] From the point view of synergistic therapy, PDT/PTT combinational therapy may enhance the therapeutic efficacy, leading to the complete eradication of tumor[30–36].

Inspired by these observations, a heavy atom-free semiconducting polymer, NDT, has been synthesized by a Stille polymerization reaction (Scheme 1). The as-obtained NDT showed a high singlet oxygen quantum yield of 21.5%. NDT nanoparticles (NPs) obtained by nanoprecipitation exhibited a

[a] *Department of Oncology, Changshu No. 2 People's Hospital, Changshu 215500, P. R. China*
[b] *Department of General Surgery, Changshu No. 2 People's Hospital, Changshu 215500, P. R. China. E-mail: chowgq0568@163.com*
[c] *Department of Materials Engineering, Changshu Institute of Technology, Changshu 215500, Jiangsu, P. R. China. E-mail: jieyang@cslg.edu.cn*
[d] *School of Pharmacy, Guilin Medical University, Guilin 541004, Guangxi, P. R. China. E-mail: zdf1226@126.com*

† Electronic supplementary information (ESI) available. See DOI: 10.1039/d1qm01236c

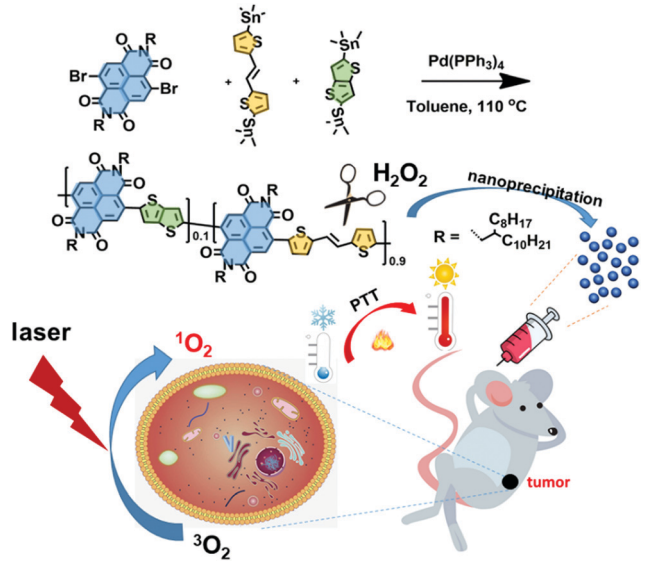

Scheme 1 Illustration of the synthesis of biodegradable NDT NPs for photothermal and photodynamic therapy.

uniform rectangle morphology with a mean diameter of ~92 nm. Owing to the high radiative transition efficiency, the photothermal conversion efficiency of such NPs is ultrahigh (65.6%). The PDT and PTT synergistic effect may promise the excellent therapeutic efficacy of NDT NPs. These NPs can be degraded in the presence of H_2O_2 in the tumor microenvironment, and they are able to target the lysosomes. The dark toxicity of such NPs is too low to be mentioned. In contrast, the phototoxicity is high enough to induce cell apoptosis with laser irradiation, and the half maximum inhibitory concentration (IC_{50}) is quite low on human cervical cells (HeLa). With the help of a laser, NDT NPs can effectively inhibit tumor growth and simultaneously cause no adverse effect on the normal tissues. Even with low power laser irradiation, complete tumor regression was observed at a low dose.

Experimental

Materials and apparatus

All chemicals were purchased from Thermal Scientific, and were used without further purification. ^{1}H NMR and ^{13}C NMR spectroscopy were performed on a Bruker DRX NMR spectrometer in $CDCl_3$ at 298 K with $CDCl_3$ as the internal standard (δ = 7.26 ppm). UV-Vis spectra were measured on a Shimadzu spectrophotometer (UV-3600 UV-Vis-NIR, Japan). The fluorescence spectra were measured on a HITACHI spectrometer (F-4600, Japan). TEM of the nanoparticles was measured on a JEOL JEM-2100 equipment. DLS was measured on a 90 Plus particle size analyzer (Brookhaven Instruments, USA).

Synthesis and characterization of NDT

4,9-Dibromo-2,7-bis(2-octyldodecyl)-benzo[*lmn*]-[3,8]-phenanthroline-1,3,6,8(2*H*,7*H*)-tetraone (197.0 mg, 0.2 mmol), 2,5-bis(trimethylstannyl)thieno-[3,2-*b*]-thiophene (9.32 mg, 0.02 mmol), and (*E*)-1,2-bis(5-(trimethylstannyl)thiophen-2-yl)-ethene (93.24 mg, 0.18 mmol) were dissolved in anhydrous toluene (5 mL), after which $Pd(PPh_3)_4$ (9.3 mg, 0.0080 mmol) was added. The solution mixture was stirred at 110 °C for 16 h under argon atmosphere. A dark solid was obtained using the same processing method as that used for NDT (180 mg). δ H 8.91–8.77 (br, 2H), 7.61–7.32 (br, 2H), 7.25–7.05 (br, 3H) 4.25–3.95 (br, 6H), 2.13–1.94(br, 2H), 1.66–1.04 (br, 64H), 0.99–0.78 (br, 12H).

Preparation of NDT NPs

The NDT NPs were prepared by nano-precipitation with DSPE-PEG_{-2000}. DSPE-PEG_{-2000} (10 mg) was dissolved in distilled water with ultrasound. Then, NDT (2 mg) was dissolved in tetrahydrofuran (THF, 1 mL). Further, 200 μL of this solution was injected into PBS using ultrasound at room temperature. After the mixture was stirred for 10 min, THF was removed by purging nitrogen.

Singlet oxygen detection

Singlet oxygen quantum yield ($^1O_2$ QY) of NDT was calculated by using DPBF (1,3-diphenylisobenzofuran) as the $^1O_2$ indicator. Generally, a mixture was prepared with the absorbance of DPBF being adjusted around 1.0 while that of NDT being 0.2 to 0.3. After irradiation for different periods of time, the absorbance spectra were recorded. The singlet oxygen quantum yield was calculated according to eqn (1).[5]

$$\Phi_{\Delta(\mathrm{NDT})} = \Phi_{\Delta(\mathrm{MB})} \times \frac{S_{\mathrm{NDT}}}{S_{\mathrm{MB}}} \times \frac{F_{\mathrm{MB}}}{F_{\mathrm{NDT}}} \quad (1)$$

Photothermal conversion efficiency of NDT NPs

NDT NPs in water was irradiated by laser and then cooled to room temperature. The temperature was recorded by an infrared camera. The photothermal conversion efficiency was calculated according to eqn (2)–(6).

$$\eta = \frac{hs(T_{\max} - T_{\mathrm{amb}}) - Q_{\mathrm{Dis}}}{I(1 - 10^{-\mathrm{A660}})} \quad (2)$$

$$\theta = \frac{T - T_{\mathrm{amb}}}{T_{\max} - T_{\mathrm{amb}}} \quad (3)$$

$$\mathrm{d}t = -\tau s\frac{\mathrm{d}\theta}{\theta} \quad (4)$$

$$\tau_s = \frac{\sum_i m_i C_{p,i}}{hs} \quad (5)$$

$$t = -\tau s \ln(\theta) \quad (6)$$

where h stands for the heat transfer coefficient and S represents the surface area of the container. $T_{\max}$ is the highest temperature of NDT NPs in water at the maximum steady-state temperature, I is the laser power density (0.5 W cm^{-2}), Q_{Dis} is the heat associated with light absorption by the solvent and A_{660} is the absorbance of the NDT NPs at 660 nm. The variable τ_s is the

sample-system time constant, and m_i and C_i are the mass and heat capacity of the deionized water (4.2×10^3 J kg^{-1} °C^{-1}), respectively.

Cell culture, cellular uptake, lysosome co-localization, MTT assay and flow cytometry

At 37 °C, human cervical cancer (HeLa) cell lines were cultured with 10% fetal bovine serum (FBS) under an atmosphere of 5% CO_2. HeLa cells were incubated with NDT NPs (15.8 μg mL^{-1}, 2 mL) in a confocal dish for different time periods in dark for 24 h. Then the medium was discarded and the cells were washed with PBS three times (1 mL). 1 mL polyoxymethylene was added for 25 min to fix the cells. Polyoxymethylene was discarded and the cells were again washed with PBS three times (1 mL). The cells were further co-cultured with lysosome tracker green (10 μmol) for 20 min. After that, the cells were washed with PBS three times (1 mL). For the cellular uptake of NDT NPs, the cells were excited at 633 nm and the fluorescence was collected from 650 to 750 nm. However, for the lysosome co-localization experiment, they were excited with a 488 nm laser, and fluorescence was collected from 490 to 560 nm.

For the MTT assay, NDT NPs were diluted with the medium to various concentrations and co-cultured with HeLa cells in a 96-well plate. For the control and illumination groups, the plate was irradiated with a laser (660 nm, 0.2 or 0.5 W cm^{-2}) for 8 minutes after 24 h culture. In contrast, the cells were not irradiated for the cells in the dark groups. Relative cell viability was then determined by MTT (3-(4,5-dimethylthiazol-2-yl)-2,5-diphenyltetrazolium bromide) assay. MTT solution (5 mg mL^{-1}, 20 μL) was added to each well followed by incubation for 4 h under the same conditions at 37 °C. Then, the solution was discarded followed by the addition of DMSO (200 μL). At ambient temperature, the absorbance was measured on a Bio-Tek microplate reader. The cell viability of the control group was considered as 100%. The relative cell viability was then calculated by the following equation:

viability (%) = mean absorbance of the group incubated with NDT NPs/mean absorbance of the group incubated without NPs.

Annexin V-FITC/propidium iodide (PI) staining

HeLa cells were plated in 6-well plates and divided into three groups (control group, dark group, and photo group). For the dark and photo groups, the cells were treated with nanoparticles at a concentration of 3.2 μg mL^{-1} and the photo group was irradiated with laser (660 nm, 0.2 or 0.5 W cm^{-2}) for 8 minutes exceptionally while the dark group was not. The apoptosis of HeLa cells was analyzed by Annexin V-FITC/propidium iodide (PI) dual staining. HeLa cells were harvested and stained with Annexin V-FITC/PI Cell Apoptosis Detection Kit (KeyGen Biotech, Nanjing, China) according to the standard protocol. The apoptosis rates of the cells were recorded on a flow cytometry equipment (BD Biosciences, San Jose, CA, USA).

In vivo photothermal imaging and phototherapy

All experiments were performed in compliance with the relevant laws and institutional guidelines. The experiments were approved by the institutional committee of Guilin Medical University (SCXK2007-001). 15 nude mice were purchased and then injected with HeLa cells into the armpit as the tumor source. These mice were divided into 3 groups at random when the tumor volume reached about 80 mm^3. For the control group, the mice were intravenously injected with PBS, while the other groups were injected with NDT NPs (200 μg mL^{-1}, 100 μL) in PBS solution, respectively. After 12 h, the tumors of the PBS + laser, NDT + laser groups were irradiated by laser (660 nm, 0.2 or 0.5 W cm^{-2}) for 8 minutes while the mice in the dark group were not irradiated. The tumor volume and body weight of mice were recorded every two days. These nude mice were sacrificed followed by the histology analysis. The main organs, including heart, liver, spleen, lung, kidney and tumor, were isolated and fixed in 4% formaldehyde solution. After dehydration, they were embedded in paraffin cassettes, and stained with hematoxylin and eosin (H&E), followed by the recording of images on a microscope.

Statistical analysis

The significance between two groups was analyzed by two-tailed Student's t-test. For multiple comparisons, one-way analysis of variance (ANOVA) with Tukey's *post hoc* test was used. Statistical analysis was performed using GraphPad Prism 6.0. P values of less than 0.05 were considered significant ($^*P < 0.05$, $^{**}P < 0.01$, $^{***}P < 0.01$).

Results and discussion

Synthesis and generation characterization of NDT

NDT was synthesized *via* a one-pot Stille coupling reaction involving 4,9-dibromo-2,7-bis(2-octyldodecyl)-benzo[lmn]-[3,8]-phenanthroline-1,3,6,8(2*H*,7*H*)-tetraone (compound **1**), 2,5-bis(trimethylstannyl)thieno-[3,2-*b*]-thiophene (compound **2**), and (*E*)-1,2-bis(5-(trimethylstannyl)thiophen-2-yl)-ethene (compound **3**) (Scheme 1). The obtained crude polymers were precipitated in methanol and then purified by Soxhlet extraction to remove the oligomers and other impurities. Specifically, NDT shows good solubility in chloroform and tetrahydrofuran at room temperature. The molecular structures of the copolymers were confirmed by ^{1}H NMR spectroscopy. First, the UV-vis and fluorescence emission spectra of NDT NPs were recorded to investigate the photophysical properties. NDT shows narrow absorption peaks at 364 and 644 nm in THF, while the emission peaks were shifted to 710 and 817 nm, respectively, indicating their ability to respond to near infrared (NIR) light (Fig. 1a and b). NDT NPs exhibit absorbance with maximum intensity at 374 and 666 nm, respectively, while the emission spectra also red shifted to 712 and 818 nm; this phenomenon was attributed to the *J*-aggregates of NDT in water. The morphology characterized by transmission electron microscopy (TEM) suggests that NDT can self-assemble into a uniform spherical morphology (Fig. 1c), which is in good agreement with the dynamic light scattering (DLS) (mean diameter ~95 nm) result (Fig. 1d).

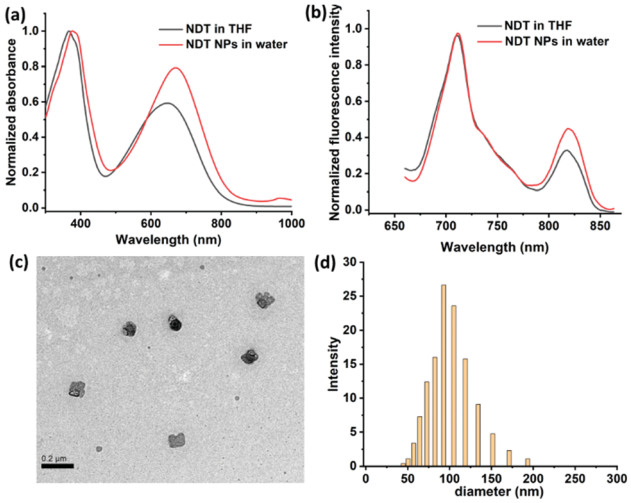

Fig. 1 (a) Normalized absorbance spectra of NDT in THF and NPs in water. (b) Normalized fluorescence spectra of NDT in THF and NPs in water. (c) TEM of NDT NPs. (d) DLS of NDT NPs in water.

Singlet oxygen generation and photothermal conversion efficiency

For an ideal photosensitizer, high singlet oxygen quantum yield ($^1O_2$ QY) is fundamental to produce enough phototoxicity to induce cell death. Therefore, the $^1O_2$ QY of NDT was determined using 1,3-diphenylisobenzofuran (DPBF) as a probe with methylene blue (MB ~ Φ = 57%) as the standard substance in DCM (Fig. S1 and S2, ESI†). The absorbance of DPBF tends to decrease with laser irradiation, indicating the efficient singlet oxygen generation of NDT. In contrast, the absorbance of NDT remained unchanged, suggesting the excellent photostability of NDT in DCM (Fig. 2a and b). The $^1O_2$ QY (21.5%) is lower than that of NDNT (55.2%),[23] DPPCz (40.3%),[24] and PTVT (42.2%).[25] It is worth noting that heavy atom-free NDT may diminish the potential dark toxicity. Further, nanoprecipitation was used to prepare NDT NPs with good dispersity in water. NDT NPs still possessed high singlet oxygen generation ability because of the photo-responsive fluorescence enhancement of singlet oxygen sensor green (SOSG), a commercially available probe (Fig. S3, ESI†). From the point view of synergistic therapy, combining PDT with PTT may achieve better therapeutic efficacy. High photothermal conversion efficiency is of tremendous significance for enhancing photothermal therapeutic efficacy. The photothermal conversion efficiency of NDT NPs was calculated by recording the heating and cooling curves in distilled water with irradiation or without irradiation (Fig. 2c and d). A temperature elevation of 42.2 °C was observed, while that of water was almost negligible (~4.8 °C). An ultrahigh photothermal conversion efficiency of NDT NPs was calculated as 65.6%, which is higher than the most of the previously reported semiconducting polymers, including NDNT NPs (40.6%),[23] DPPCz NPs (48.2%),[24] and PTVT NPs (52.6%).[25] After irradiation, the absorbance spectra were recorded for comparison. These NPs showed excellent photostability because no obvious

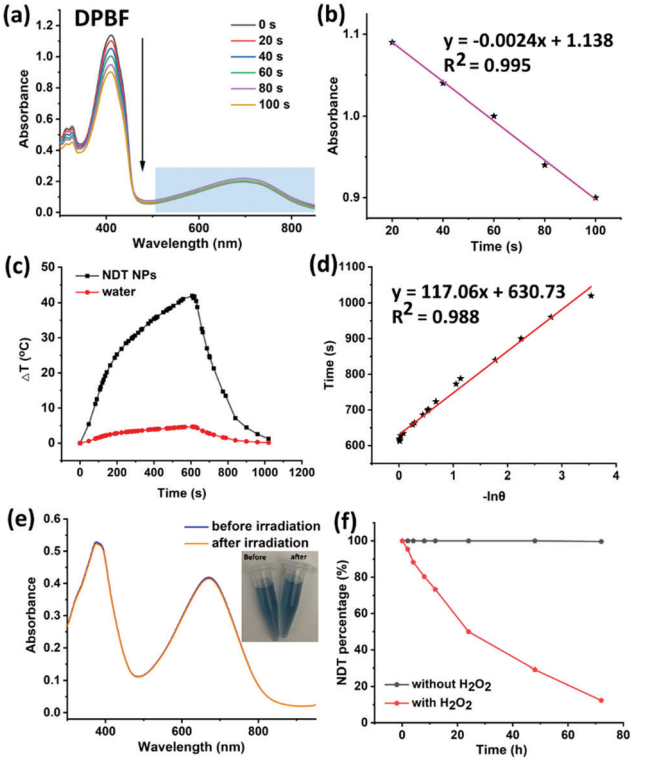

Fig. 2 (a) $^1O_2$ generation of NDT with DPBF as a probe in DCM. (b) Linear fitting of time *versus* absorbance. (c) Heating and cooling curve of NDT NPs with or without irradiation. (d) Linear fitting of lnθ *versus* time. (e) Absorbance of NDT NPs in water before and after irradiation. (f) Degradation of NDT NPs by recording the absorbance in the presence of H_2O_2.

decay was observed, regardless of being irradiated or not (Fig. 2e).

Tumor microenvironment (TME) features high H_2O_2 concentration. Due to the fact that C=C double bonds in thiophene can react with H_2O_2, the absorbance of NDT NPs was recorded in the presence of H_2O_2 to investigate the degradation of NDT NPs *in vitro*. As shown in Fig. 2f, the absorbance of NDT NPs kept decreasing and over 80% degradation rate was observed after 3 days, indicating that these NPs would be bio-degradable in TME.

Cellular uptake, lysosome co-localization, MTT assay and flow cytometry *in vitro*

Since the singlet oxygen and photothermal conversion efficiency of NDT NPs were high, we then evaluated the therapeutic efficacy of NDT NPs *in vitro* on HeLa cells. First, confocal laser scanning microscopy (CLSM) was used to investigate the cellular uptake and singlet oxygen generation of NDT NPs. As shown in Fig. 3a, NDT NPs could be uptaken by HeLa cells (red channel), and these NPs could accumulate in the lysosomes (green channel). The cytotoxicity of NDT NPs was investigated by MTT assay. Negligible dark toxicity was observed, as indicated by the high cell viability without irradiation (Fig. 3b and c). Concentration dependent phototoxicity indicated that these NPs were able to kill HeLa cells with irradiation (Fig. 3b and c).

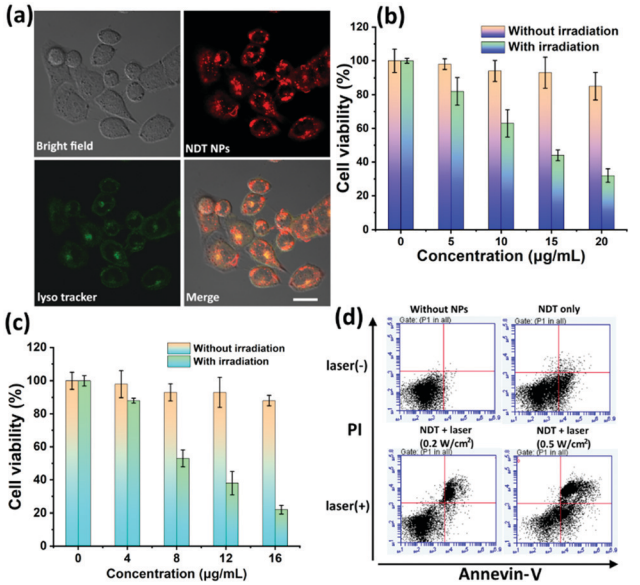

Fig. 3 (a) Cellular uptake of NDT NPs in HeLa cells and lysosome co-localization with a lysosome tracker. (b) MTT assay of NDT NPs with or without laser irradiation (660 nm, 0.2 W cm^{-2}). (c) MTT assay of NDT NPs with or without laser irradiation (660 nm, 0.5 W cm^{-2}). (d) Flow cytometry experiment of NPs with or without laser irradiation.

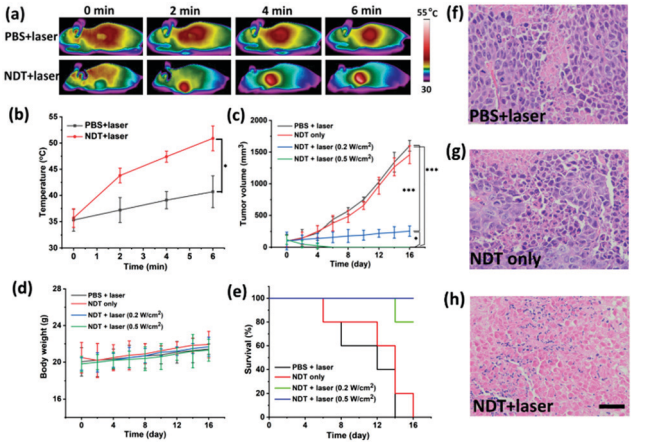

Fig. 4 (a) Time dependent photothermal imaging of HeLa tumor bearing mice injected with NDT NPs. (b) Quantification of the tumor temperature at different time points. (c) Tumor volume of the mice in the PBS + laser, NDT only and NDT + laser groups (0.2 or 0.5 W cm^{-2}). (d) Body weight change. (e) Survival rate of the mice in the PBS + laser, NDT only and NDT + laser groups. (f–h) H&E-stained pictures of the tumor in the PBS + laser and NDT only and NDT + laser (0.2 W cm^{-2}) groups.

With the increase of the laser power, a lower half maximal inhibitory concentration was observed; this phenomenon could be ascribed to the synergistic effect of PDT and PTT (Fig. 3b and c). Cell viability remained very high, even though the concentration of NDT was as high as 200 μg mL^{-1}, suggesting the low dark toxicity of NDT NPs (Fig. S4, ESI†). Further, flow cytometry was also used to investigate cell apoptosis with or without laser irradiation; the results were consistent with the MTT assay. In the control group, a high cell viability was observed. For the dark group, NDT NPs showed negligible toxicity, while the apoptotic rate was enhanced with the increase of the power density of the laser (Fig. 3d).

In vivo photothermal imaging and phototherapy

Considering the high phototoxicity of NDT NPs *in vitro*, we further investigated the PDT and PTT synergistic therapeutic efficacy *in vivo*. Photothermal imaging was used to quantify the temperature of the tumor with laser irradiation (Fig. 4a and b). When the tumor volume of 3 nude mice reached 200 mm^3, these mice were intravenously injected with NDT NPs. After 12 h, the tumor was irradiated with laser (660 nm, 0.5 W cm^{-2}). The temperature was recorded using an infrared camera. For the control group, almost negligible temperature elevation was observed, while the tumor temperature reached 51.3 °C for those injected with NDT NPs, indicating the excellent photothermal therapeutic efficacy. For the control and NDT only group, the tumor grew at a parallel speed, suggesting the low dark toxicity of the NPs. For the irradiation group, the tumor proliferation was inhibited effectively even at 0.2 W cm^{-2}. Further, tumor suppression was observed at a higher power density (0.5 W cm^{-2}) (Fig. 3c). After treating twice, the tumors disappeared, mainly because of the PDT and PTT synergistic effect. No obvious body weight change was observed, demonstrating the low toxicity of these NPs (Fig. 3d). The survival also demonstrated the excellent biocompatibility of these NPs. These mice were then sacrificed, and the H&E-stained pictures of the tumors in PBS + laser, NDT only and NDT + laser groups are illustrated in Fig. 4f–h. The morphology of the nucleus in the PBS + laser and NDT only group remained in good manner, while that in the NDT + laser group was damaged, indicating the low dark toxicity and high phototoxicity of these NPs.

After treatment, all mice were sacrificed, followed by the collection of the normal organs, including heart, liver, spleen, lung and kidneys. The representative tumor pictures in each group are illustrated in Fig. S5 (ESI†). The hematological parameters, liver and renal function were investigated by recording the white blood cell, red blood cell, aspartate aminotransferase, alanine aminotransferase, total protein and blood urea nitrogen (Fig. 5a–f and Table S1, ESI†). The parameters in the dark and photo groups were in good agreement with those of the control groups, indicating that the mice were very healthy. Further, no obvious difference was observed in the H&E-stained pictures of the normal organs in the three groups (Fig. 6), demonstrating that NDT NPs exerted no side effects *in vivo*, suggesting their excellent bio-compatibility.

Conclusions

In summary, a semiconducting polymer photosensitizer NDT with ultrahigh photothermal conversion efficiency (~65.6%) has been designed and prepared. NDT NPs obtained by nanoprecipitation were capable of responding to the excess H_2O_2 in the tumor microenvironment, leading to the biodegradation of the NPs. NDT NPs showed considerably high phototoxicity as well as negligible dark toxicity towards HeLa cells. *In vivo*

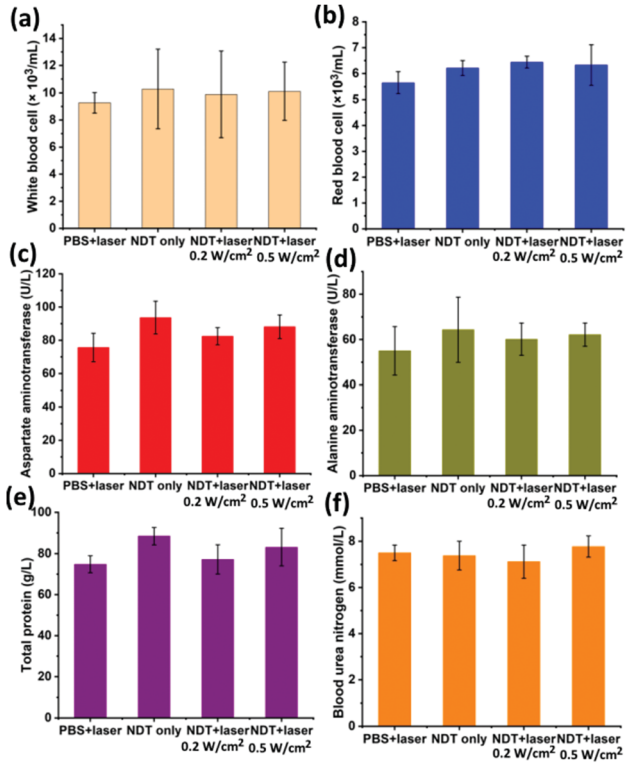

Fig. 5 (a) White blood cell. (b) Red blood cell. (c) Aspartate aminotransferase. (d) Alanine aminotransferase. (e) Total protein. (f) Blood urea nitrogen of the mice in PBS + laser, NDT only, NDT + laser (0.2 or 0.5 W cm^{-2}) groups.

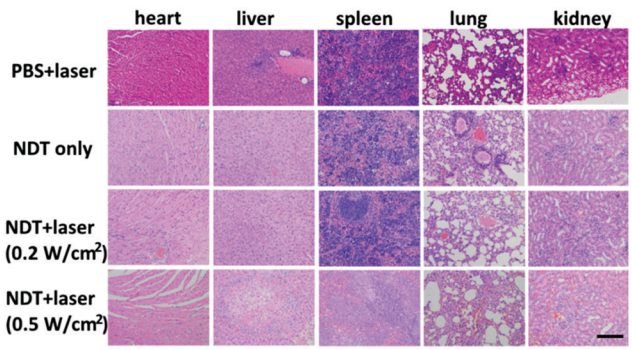

Fig. 6 H&E pictures of heart, liver, lung, kidney and spleen in the PBS + laser, NDT only and NDT + laser groups (0.2 or 0.5 W cm^{-2}). Scale bar: 10 μm.

photothermal imaging and phototherapy suggests that these NPs could inhibit tumor growth at a low dose. Owing to the PDT and PTT synergistic effect, complete tumor suppression was achieved. However, no damage was caused to normal tissues, suggesting the biocompatibility of these NPs. These results provide a way to design heavy atom-free semiconducting photosensitizers with low dark toxicity, high phototoxicity and good biocompatibility for photothermal and photodynamic therapy.

Conflicts of interest

The authors have no conflict of interest to declare.

Acknowledgements

The authors acknowledge the financial support from the National Science Foundation of the Jiangsu Higher Education Institutions of China (No. 20KJA430006) and the Six Talent Peaks Project of Jiangsu Province (No. 2018-SWYY-001).

Notes and references

1 R. L. Siegel, K. D. Miller, H. E. Fuchs and A. Jemal, Cancer Statistics, 2021, *Ca-Cancer J. Clin.*, 2021, **71**(1), 7–33.
2 Z. Zhou, J. Song, L. Nie and X. Chen, Reactive oxygen species generating systems meeting challenges of photodynamic cancer therapy, *Chem. Soc. Rev.*, 2016, **45**(23), 6597–6626.
3 L. Li, J. Zou, Y. Dai, W. Fan, G. Niu, Z. Yang and X. Chen, Burst release of encapsulated annexin A5 in tumours boosts cytotoxic T-cell responses by blocking the phagocytosis of apoptotic cells, *Nat. Biomed. Eng.*, 2020, **4**(11), 1102–1116.
4 J. Li, D. Cui, Y. Jiang, J. Huang, P. Cheng and K. Pu, Near-Infrared Photoactivatable Semiconducting Polymer Nanoblockaders for Metastasis-Inhibited Combination Cancer Therapy, *Adv. Mater.*, 2019, **31**(46), e1905091.
5 J. Zou, L. Li, J. Zhu, X. Li, Z. Yang, W. Huang and X. Chen, Singlet oxygen "afterglow" therapy with NIR-II fluorescenct molecules, *Adv. Mater.*, 2021, **33**, 2103627.
6 J. Zou, L. Li, Z. Yang and X. Chen, Phototherapy meets immunotherapy: a win-win strategy to fight against cancer, *Nanophotonics*, 2021, **10**(12), 3229–3245.
7 Z. Meng, X. Zhou, J. Xu, X. Han, Z. Dong, H. Wang, Y. Zhang, J. She, L. Xu, C. Wang and Z. Liu, Light-Triggered In Situ Gelation to Enable Robust Photodynamic-Immunotherapy by Repeated Stimulations, *Adv. Mater.*, 2019, **31**(24), e1900927.
8 J. Zou, Z. Yin, P. Wang, D. Chen, J. Shao, Q. Zhang, L. Sun, W. Huang and X. Dong, Photosensitizer synergistic effects: D-A-D structured organic molecule with enhanced fluorescence and singlet oxygen quantum yield for photodynamic therapy, *Chem. Sci.*, 2018, **9**, 2188–2194.
9 Y. Liu, P. Bhattarai, Z. Dai and X. Chen, Photothermal therapy and photoacoustic imaging via nanotheranostics in fighting cancer, *Chem. Soc. Rev.*, 2019, **48**(7), 2053–2108.
10 Q. Chen, Q. Hu, E. Dukhovlinova, G. Chen, S. Ahn, C. Wang, E. A. Ogunnaike, F. S. Ligler, G. Dotti and Z. Gu, Photothermal Therapy Promotes Tumor Infiltration and Antitumor Activity of CAR T Cells, *Adv. Mater.*, 2019, **31**(23), e1900192.
11 Y. Ma, Y. Zhang, X. Li, Y. Zhao, M. Li, W. Jiang, X. Tang, J. Dou, L. Lu, F. Wang and Y. Wang, Near-Infrared II Phototherapy Induces Deep Tissue Immunogenic Cell Death and Potentiates Cancer Immunotherapy, *ACS Nano*, 2019, **13**(10), 11967–11980.
12 J. Li, J. Huang, Y. Lyu, J. Huang, Y. Jiang, C. Xie and K. Pu, Photoactivatable Organic Semiconducting Pro-nanoenzymes, *J. Am. Chem. Soc.*, 2019, **141**(9), 4073–4079.

13 J. Li, D. Cui, J. Huang, S. He, Z. Yang, Y. Zhang, Y. Luo and K. Pu, Organic Semiconducting Pro-nanostimulants for Near-Infrared Photoactivatable Cancer Immunotherapy, *Angew. Chem., Int. Ed.*, 2019, **58**(36), 12680–12687.

14 Q. Lu, S. Qi, P. Li, L. Yang, S. Yang, Y. Wang, Y. Cheng, Y. Song, S. Wang, F. Tan and N. Li, Photothermally activatable PDA immune nanomedicine combined with PD-L1 checkpoint blockade for antimetastatic cancer photoimmunotherapy, *J. Mater. Chem. B*, 2019, **7**, 2499–2511.

15 M. Chang, Z. Hou, M. Wang, M. Wang, P. Dang, J. Liu, M. Shu, B. Ding, A. A. Al Kheraif, C. Li and J. Lin, Cu_2MoS_4/Au Heterostructures with Enhanced Catalase-Like Activity and Photoconversion Efficiency for Primary/Metastatic Tumors Eradication by Phototherapy-Induced Immunotherapy, *Small*, 2020, **16**, e1907146.

16 J. Zhu, J. Zou, J. Zhang, Y. Sun, X. Dong and Q. Zhang, An anthracene functionalized BODIPY derivative with singlet oxygen storage ability for photothermal and continuous photodynamic synergistic therapy, *J. Mater. Chem. B*, 2019, **7**(20), 3303–3309.

17 J. Zou, P. Wang, Y. Wang, G. Liu, Y. Zhang, Q. Zhang, J. Shao, W. Si, W. Huang and X. Dong, Penetration depth tunable BODIPY derivatives for pH triggered enhanced photothermal/photodynamic synergistic therapy, *Chem. Sci.*, 2019, **10**, 268–276.

18 M. Wang, J. Song, F. Zhou, A. R. Hoover, C. Murray, B. Zhou, L. Wang, J. Qu and W. R. Chen, NIR-Triggered Phototherapy and Immunotherapy via an Antigen-Capturing Nanoplatform for Metastatic Cancer Treatment, *Adv. Sci.*, 2019, **6**(10), 1802157.

19 D. Xu, J. Liu, Y. Wang, Y. Jian, W. Wu and R. Lv, Black Phosphorus Nanosheet with High Thermal Conversion Efficiency for Photodynamic/Photothermal/Immunotherapy, *ACS Biomater. Sci. Eng.*, 2020, **6**(9), 4940–4948.

20 X. Zhang, J. Tang, C. Li, Y. Lu, L. Cheng and J. Liu, A targeting black phosphorus nanoparticle based immune cells nano-regulator for photodynamic/photothermal and photo-immunotherapy, *Bioact. Mater.*, 2021, **6**, 472–489.

21 W. Ou, L. Jiang, R. K. Thapa, Z. C. Soe, K. Poudel, J. H. Chang, S. K. Ku, H. G. Choi, C. S. Yong and J. O. Kim, Combination of NIR therapy and regulatory T cell modulation using layer-by-layer hybrid nanoparticles for effective cancer photoimmunotherapy, *Theranostics*, 2018, **8**, 4574–4590.

22 S. Qi, L. Lu, F. Zhou, Y. Chen, M. Xu, L. Chen, X. Yu, W. R. Chen and Z. Zhang, Neutrophil infiltration and whole-cell vaccine elicited by N-dihydrogalactochitosan combined with NIR phototherapy to enhance antitumor immune response and T cell immune memory, *Theranostics*, 2020, **10**, 1814–1832.

23 J. Shen, J. Chen, Z. Ke, D. Zou, L. Sun and J. Zou, Heavy atom-free semiconducting polymer with high singlet oxygen quantum yield for prostate cancer synergistic phototherapy, *Mater. Chem. Front.*, 2019, **3**(6), 1123–1127.

24 J. Deng, N. Zhong, X. Zhang, C. Li, C. Xu and J. Zhao, A carbazole functionalized semiconducting compound as a heavy atom free photosensitizer for phototherapy against lung cancer, *J. Mater. Chem. B*, 2020, **8**(47), 10764–10769.

25 X. Zhang, A. Zhang, J. Feng, J. Yi, L. Peng, J. Chen, Z. Ke, J. Yang, Y. Dai and D. Zou, A heavy atom free semiconducting polymer with high singlet oxygen quantum yield for photodynamic and photothermal synergistic therapy, *Mater. Des.*, 2021, 197.

26 Z. Yang, W. Fan, J. Zou, W. Tang, L. Li, L. He, Z. Shen, Z. Wang, O. Jacobson, M. Aronova, P. Rong, J. Song, W. Wang and X. Chen, Precision Cancer Theranostic Platform by In Situ Polymerization in Perylene Diimide-Hybridized Hollow Mesoporous Organosilica Nanoparticles, *J. Am. Chem. Soc.*, 2019, **141**, 14687–14698.

27 J. Zou, J. Zhu, Z. Yang, L. Li, W. Fan, L. He, W. Tang, L. Deng, J. Mu, Y. Ma, Y. Cheng, W. Huang, X. Dong and X. Chen, A Phototheranostic Strategy to Continuously Deliver Singlet Oxygen in the Dark and Hypoxic Tumor Microenvironment, *Angew. Chem., Int. Ed.*, 2020, **59**(23), 8833–8838.

28 W. Tang, Z. Yang, S. Wang, Z. Wang, J. Song, G. Yu, W. Fan, Y. Dai, J. Wang, L. Shan, G. Niu, Q. Fan and X. Chen, Organic Semiconducting Photoacoustic Nanodroplets for Laser-Activatable Ultrasound Imaging and Combinational Cancer Therapy, *ACS Nano*, 2018, **12**(3), 2610–2622.

29 J. Li, D. Cui, Y. Jiang, J. Huang, P. Cheng and K. Pu, Near-Infrared Photoactivatable Semiconducting Polymer Nanoblockaders for Metastasis-Inhibited Combination Cancer Therapy, *Adv. Mater.*, 2019, **31**, e1905091.

30 L. Chen, L. Zhou, C. Wang, Y. Han, Y. Lu, J. Liu, X. Hu, T. Yao, Y. Lin, S. Liang, S. Shi and C. Dong, Tumor-Targeted Drug and CpG Delivery System for Phototherapy and Docetaxel-Enhanced Immunotherapy with Polarization toward M1-Type Macrophages on Triple Negative Breast Cancers, *Adv. Mater.*, 2019, **31**, e1904997.

31 J. Chi, Q. Ma, Z. Shen, C. Ma, W. Zhu, S. Han, Y. Liang, J. Cao and Y. Sun, Targeted nanocarriers based on iodinated-cyanine dyes as immunomodulators for synergistic phototherapy, *Nanoscale*, 2020, **12**, 11008–11025.

32 C. Wu, X. Guan, J. Xu, Y. Zhang, Q. Liu, Y. Tian, S. Li, X. Qin, H. Yang and Y. Liu, Highly efficient cascading synergy of cancer photo-immunotherapy enabled by engineered graphene quantum dots/photosensitizer/CpG oligonucleotides hybrid nanotheranostics, *Biomaterials*, 2019, **205**, 106–119.

33 X. Zhang, J. Tang, C. Li, Y. Lu, L. Cheng and J. Liu, A targeting black phosphorus nanoparticle based immune cells nano-regulator for photodynamic/photothermal and photo-immunotherapy, *Bioact. Mater.*, 2021, **6**, 472–489.

34 L. Zhou, L. Chen, X. Hu, Y. Lu, W. Liu, Y. Sun, T. Yao, C. Dong and S. Shi, A Cu_9S_5 nanoparticle-based CpG delivery system for synergistic photothermal-, photodynamic- and immunotherapy, *Commun. Biol.*, 2020, **3**, 343.

35 Y. Zhou, S. Liu, C. Hu, L. Cai and M. Pang, A covalent organic framework as a nanocarrier for synergistic phototherapy and immunotherapy, *J. Mater. Chem. B*, 2020, **8**, 5451–5459.

36 Y. Zhu, J. Xue, W. Chen, S. Bai, T. Zheng, C. He, Z. Guo, M. Jiang, G. Du and X. Sun, Albumin-biomineralized nanoparticles to synergize phototherapy and immunotherapy against melanoma, *J. Controlled Release*, 2020, **322**, 300–311.

